Research Article

Filippo Giammaria Praticò, Diana Severini*, and Pasquale Giuseppe Fabio Filianoti

Can sensor-based noise mapping be a proxy of PM and permeability mapping?

https://doi.org/10.1515/noise-2021-0024
Received May 11, 2021; accepted Nov 09, 2021

Abstract: In recent decades, road infrastructures have been the subject of numerous studies, aimed at ensuring reduced air and acoustic pollution. On the other hand, several studies showed that another important problem is dust load. Indeed, for internal combustion engine (ICEVs) and electric vehicles (EVs), suspended solids, fine particles, heavy metals, nutrients and organic chemicals can lead to a gradual reduction in terms of drainage characteristics, negatively affecting road acoustic characteristics. The purpose of this study is to discuss if sensor-based noise mapping can be a proxy of particulate matter (PM) and permeability mapping. More precisely, the main objective of this study is to discuss conceptual analogies among noise, PM, and permeability mapping. Selected specimens were produced with and without crumb rubber.

Keywords: low-noise mixtures, electric vehicles, dust load, acoustics, permeability, clogging

1 Introduction

Over the last thirty years, many road infrastructure studies aimed at reducing environmental impacts, ensuring safe circulation, reducing noise and vibration induced by rolling, as well as energy consumption, related to tyre-road interaction. Noise mapping is a crucial part of these efforts (cf. Figure 1) where pavement characteristics and traffic play an outstanding role (absorption and propagation), synergistically affecting acoustics, pollution, and pavement permeability. Noise maps are set up by European cities with more than 100.000 inhabitants every 5 years. The standard references include the CNOSSOS-EU and the directive 2015/996 (cf. [1] and [2]). The importance of noise maps from many points of view has been pointed out and discussed in the literature (*e.g.*, [3]).

For Pollution, note that while traditional vehicles use internal combustion engines (ICEVs) and fossil fuels (i.e., gasoline or diesel, with concerned emissions such as carbon dioxide, hydrocarbons, carbon monoxide, carbon monoxide, and nitrogen oxides [4]), electric vehicles may imply energy savings and emission reduction [4] (reduction of CO_2 VOC, NO_x, and SO_2 [5]). Note that EVs could emit the same amount of PM10 and $PM_{2.5}$ [6] (non-exhaust emissions) as gasoline and diesel cars, while being as noisy as ICEs at high speeds [7–11].

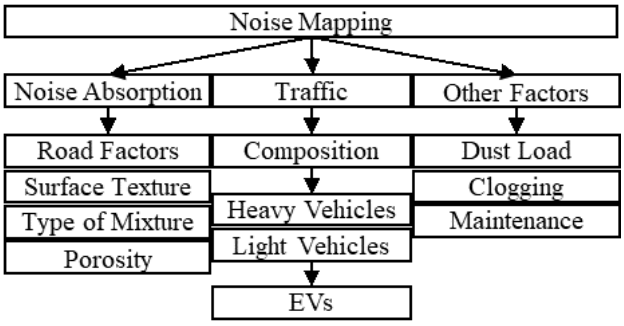

Figure 1: Noise mapping-related variables

For pollution, note that road traffic is one of the most significant sources of air pollution (cf. Figure 1), where meteorological conditions, fossil fuels, gas emissions, and vehicles interact (mechanical components of cars, brakes, pads, speeds, operating conditions of the vehicle, vehicle weight [6]). Polluting particles can be divided into exhaust

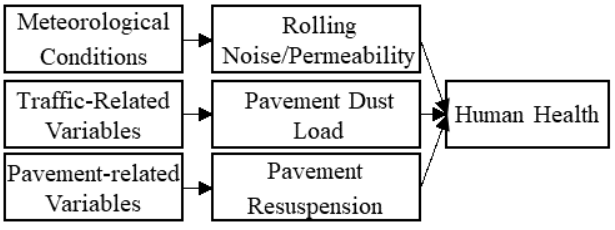

Figure 2: Variables that affect human health

***Corresponding Author: Diana Severini:** University Mediterranea of Reggio Calabria, Reggio Calabria, Italy;
Email: diana.severini@unirc.it
Filippo Giammaria Praticò, Pasquale Giuseppe Fabio Filianoti: University Mediterranea of Reggio Calabria, Reggio Calabria, Italy

Table 1: Sources, gradation, effects on human health of chemical elements

Chemical elements	Sensor/device	Reference
Zn, Ni, Cu, Pb, Fe	Inductively coupled plasma mass spectrometry	[15]
Si, Cr, Pb, Fe, Ti, V, Al, Cl	X-ray fluorescence	USEPA, 2014
Zn, Si, Tl, Cr, Ni, Cu, Sb, Pb, Ba, Fe, Ti, Zr, Sn, V, Sr, Al, K, Ca, Mg, Cd, As, Mn, Rb	Atomic absorption spectroscopy	https://web.nmsu.edu/~esevosti/report.htm
Zn, Cu, Pb	Catalytic DNA sensors	https://www.quasarinstruments.com/
Cr, Ni, Zr, Rb	Inductively coupled plasma atomic emission spectroscopy	https://www.ssi.shimadzu.com/industry/environmental/icp-aes.html
Zn, Si, Tl, Cr, Cu, Sb, Pb, Ba, Fe, Ti, Zr, Sn, V, Sr, Al, K, Ca, Mg, Cd, As,	Inductively coupled plasma optical emission spectrometry	https://www.quasarinstruments.com/
Ni	Electrochemical voltammetric analyzer	https://www.sinsilinternational.com/Electrochemical-Analyzer.html
Pb, Cl	Energy Dispersive X-ray Fluorescence	https://www.rigakuedxrf.com/petroleum.php
Cd, Cu, Fe, Ni, Zn	Spectrofluorometer fluorescence biosensor	[16]

Table 2: Sensors that can be used to detect chemical elements

Cause	Gradation	Human health effects	Chemical elements	Reference
Tire wear	2.5–10 μm	Respiratory disease	Zn, Cu, Sb, Pb	[17]
	2.5 μm and smaller	Cancer	Si, Tl, Cr, Ni	[17]
		Cardiovascular disease	Ba, Fe, Ti, Zr, Sn, V, Sr, Al	[17]
Brake wear	60–70 nm or less	Kidney problems	Cu, Ba, Zn, Fe, Sb, K, Ti	[17]
	0.2–10 μm	Bone problems	Pb, Zr	[17]
		Neurobehavioral disorders		
		Lung cancer		
Road traffic	25–70 nm	Respiratory disease	Si, Al, Ca, Mg, Fe	[17]
		Cancer		
Road dust	10 μm and smaller	Respiratory disease	Cl, Pb, Cd, Zn	[17]
		Cancer	As, Ba, Cr, Cu, Fe, Mn, Ni, Ti	[17]
			Zr, Rb, Sr	[17]
Fuel (gasoline and diesel)	2–120 nm 40–80 nm	Irritation of mucous, throat and lungs	S, Zn	[17]
Road surface	6-25 μm	Cardiovascular disease	Zn, Cr, Ni, Pb, As, Ti, V	[17]
		Cancer	Ca	[18]

emissions and non-exhaust emissions [12, 13], where primary particles are directly released into the atmosphere by human or natural sources, and secondary particles are generated by mechanical or chemical reactions and can be classified in terms of aerodynamic diameter [13].

Non-exhaust traffic emissions are the major source of dust load [12]. The dust load is the total amount of dust available on a given surface and is affected by the resuspension of road dust. Table 1 analyses the different sources of pollutants related to the road pavement, also indicating their size and their possible effects on human health [14]. Table 2 shows the sensors that can be used to detect them and quantifies their concentration.

Several studies have already shown the correlation between the exposure to particulate matter and the onset of acute and/or chronic symptoms, which undermine

Table 3: Risk related to chemical elements

Chemical elements	Concentration C [mg/kg]	Hazard quotient HQ		Reference	Risk
Zn	649.61	0.004	Negligibile	[17]	2.47
Cr	101.47	0.170	Negligibile		17.25
Ni	52.84	0.005	Negligibile		0.25
Cu	167.03	0.007	Negligibile		1.12
Pb	226.85	0.120	Negligibile		27.22
Ba	265.51	0.010	Negligibile		2.52
As	10.11	0.052	Negligibile		0.53
Mn	398.46	0.033	Negligibile		13.15
Sr	75.74	0.001	Negligibile		0.04

the health of the exposed population: cardiovascular, cerebrovascular and respiratory mortality, lung cancer [14]. A value that can be taken into consideration to assess the risk due to exposure to pollutants is the hazard quotient (HQ). This is the ratio of the potential exposure to a substance and the level at which no adverse effects are expected. A hazard quotient less than or equal to 1 indicates that adverse effects are not likely to occur (negligible hazard, https://www.chemsafetypro.com). The risk, R, related to the concentration and exposure to the chemical elements present in the study [17] is calculated through the following expression:

$$R = C \cdot HQ \tag{1}$$

where C stands for concentration (mg/kg) of the elements present in street dust and HQ is the Hazard quotient derived from the same author. Analysing Table 3, it can be noted that Pb, Cr, Mn, Ba, Zn and Cu have the greatest values of risk.

The dust load ranges from a few grams to several hundred grams per day and m^2 [19, 20].

There are different methods for quantifying road dust and its suspension, such as mobile and stationary methods. The mobile measurements platforms SNIFFER [21] and TRAKER [22] allow for measurements of road dust collected from behind the tyre in a tube, also recording speed, acceleration and direction of travel. This happens thanks to an onboard GPS [22] (this type of platforms may overestimate the concentration of the smallest particles).

The brushing or sweeping method is stationary. The sweeping operations can be carried out manually or using a vacuum sweeping machine.

In this case, the vacuum hose is hydrated with water, depending on atmospheric conditions, to avoid dispersing the particles into the air [19]. The resulting material is then collected in plastic bags, sieved and analysed [23]. The collected material is placed in a suspension chamber and then scattered using compressed air. The PM10 material is then hit by airflow in a virtual impactor, where the separation of the PM2.5 takes place (it is deposited on a membrane filter [23]). The filters are then weighed and analysed [24]. For the analyses, in [25], ICP-MS (inductively coupled plasma – optical emission spectrometer) and ICP-AES (Inductively Coupled Plasma Atomic Emission Spectrometry) were used.

A stationary device that can be used both in dry and wet conditions is the wet dust sampler (WDS), which can collect all the particles available on the surface. The WDS was developed at the Swedish National Road and Transport Research Institute (VTI) [26] and it uses a high-pressure washing of a small, defined-sized, sample surface (0.002043 m^2, [20]). The area is sealed by a^n operator standing on the foot plate, thus pressing a circular cellular rubber ring against the surface. The water, containing road dust, is then transferred into a sampling bottle using filtered compressed air. Consequently, the water can be analysed.

The VTI Road Simulator is a driving simulator designed and built at the Swedish National Road and Transport Research Institute (VTI). The simulator has 4 wheels that rotate on a circular test track with a diameter of 5.3 m [12], whose pavement and tyres can be chosen and tested for wear, also controlling both temperature and humidity. This research tool is used to generate wear particles without considering the contribution due to the surrounding environment [12]. Particles are usually analysed using a particle sizer.

For the acoustic characterisation of road pavements, different concepts may be applied, including:

- The Statistical Pass-By Method (SPB, ISO 11819-1);
- The ADRIENNE method (ISO 13472-1:2004);
- The Close Proximity method (CPX, ISO 11819-2:2011);
- The sound absorption coefficient (Kundt tube Type, ISO 10534-2: 1998, Figure 5);

- The *in situ* testing on low absorption pavements (ISO 13472-2:2010).

There are many devices instruments available in the literature for measuring permeability values, including [27]):

- The Flexible Wall Permeameter (falling-head permeameter, ASTM PS-129, withdrawn in 2003, FM 5-565);
- The Belgian Permeameter (CME 54.10);
- The "Autostrade" permeameter (Società Autostrade 2001 requirements);
- The NCAT Asphalt Field Permeameter (National Center for Asphalt Technology (NCAT), [28, 29]).

Finally, the pavement quality indicator (PQI; see Figure 7) device is an *in situ* instrument used to make real time measurements of asphalt pavement density though a non-destructive and non-nuclear method. The PQI device is made up of a transmitter, an isolation ring and a receiver.

Figure 3: ADRIENNE method

(a)

(b)

Figure 4: Kundt tube (a); Microphones (b)

Figure 5: Flexible Wall Permeameter

Figure 6: NCAT Asphalt Field Permeameter

Figure 7: PQI device

2 Objectives

The main objective of this study is to discuss conceptual analogies among noise, particulate matter (PM), and permeability mapping. Experiments and analyses were organised in tasks as follows (Figure 9):

– Task 1: Analysis of the literature and design of experiments.

- Task 2. Production of samples through the Superpave gyratory compactor. Three of them contained crumb rubber and three ones did not. The percentage of bitumen was changed accordingly.
- Task 3: Tests on samples (mechanical impedance, sound absorption coefficient, airflow resistance, bulk specific gravity, permeability, skid resistance, sand patch).
- Task 4: Data analysis, modelling, and conclusions.

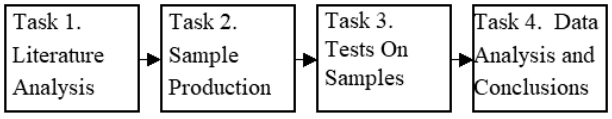

Figure 8: Experiments and analyses organised in tasks

The remaining parts of the paper are organized as follows. Section 3 deals with the characterization of the mixtures (equipment to use and proposed strategies are discussed). In Section 4 the results are discussed. Section 5 focuses on the connection between the main parameters of the tests and, finally, in Section 6 conclusion are drawn.

3 Methods and materials

Table 4 and Figures 9–11 refer to the design of experiments. By referring to samples and tests, note that due to the need to carry out different tests through very different pieces of equipment, a preliminary analysis was carried out to assess the optimal dimension to have for the samples, in order to comply with the different test requirements. Table 4 summarises the required dimensions of samples according to the different tests.

On the basis of the abovementioned characteristics, 9 specimens were produced with a diameter of 97.5 mm and an average height of 64 mm. Three samples with crumb rubber and three without were produced, with three different percentages of bitumen. The samples were compacted through the Superpave Giratory Compactor (cf. Figure 11b) (AASHTO T-312 and UNI EN 12697-31), at N_{des} = 75 (as an intermediate value between 50 and 120) and at N_{des} = 50 (ANAS requirements [30]).

For each specimen, the following parameters were determined:

1. Mechanical impedance (impulse hammer, cf. EN 29052-1, ISO 7626-5, Figure 11c). An Impulse Hammer (cf. EN 29052-1 and ISO 7626-5) was used. The impulse hammer is equipped with an integrated piezoelectric

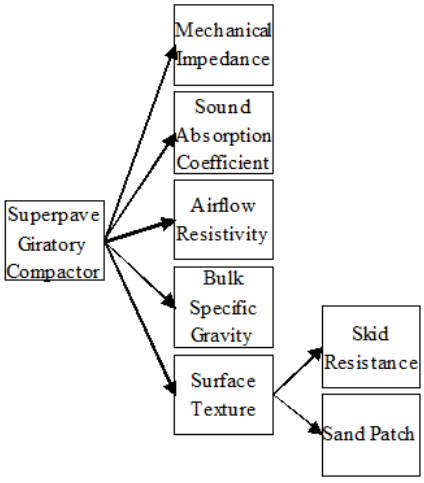

Figure 9: Processes and parameters

Table 4: Geometric characteristics of the specimen for device

Devices and standards	Geometrical characteristics	
	Diameter [mm]	Height [mm]
1. Superpave giratory compactor AASHTO T-312, UNI EN 12697-31	100	(0,66-1.05)*D (1)
2. Impulse hammer EN 29052-1, ISO 7626-5	-	-
3. Kundt tube ISO 10534-2, ASTM E1050-12	97.5	225 (2)
4. Nor1517A UNI EN ISO 9053-1, ASTM C522-03	100	225 (2)
5. Corelok ASTM D6752-02, AASHTO T-331	100	-
6. Pendulum tester EN 13036-4	-	-
7. Sand patch test EN 13036-1, ASTM E965	-	-
8. Laser profilometers ISO 13473-3	-	-
9. Flexible wall permeameter ASTM PS 129-1	(≈) 100	100 (2)

Notes. (1) Minimum height value of compacted specimen, corresponding to a zero percentage of voids, according to the standard EN 12697-31. (2) Maximum height.

force sensor and records the applied force. The force sensor is located right after the so-called "Kalotte" (front part), which brings the impact pulse on the system. The response of the impact pulse is determined by an accelerometer in the form of a frequency-dependent signal. During the measurement the load-time functions of signals (input and output signal) are sent to the computer.

2. Sound absorption coefficient (impedance tube, cf. ISO 10534-2, ASTM E1050-12, [31], Figure 4a). After being compacted, the samples were tested for the sound absorption, using the transfer-function method, according to the ISO 10534-2. Each specimen, prior to being inserted into the impedance tube, was laterally sealed using sheaths, while the top was sealed using some mouldable clay (Figure 11h).
3. Airflow resistivity (Nor1517A, cf. UNI EN ISO 9053-1, ASTM C522-03, Figure 11d). Subsequently, each sample (Figure 11i) was placed into the apparatus Norsonic Nor1517A to measure the Airflow Resistance, by applying the airflow method B in accordance with the EN ISO 9053-1. The test procedure provides for placing a cylindrical specimen into a sample holder that closes the open end of a vessel with known volume and diameter. A piston generates a slowly alternating airflow through the test specimen. The alternating component of the test pressure is measured by the microphone and the sound level meter.
4. Bulk specific gravity (automatic vacuum sealing method, cf. ASTM D6752-02, AASHTO T-331, Figure 11e). The Automatic Vacuum Sealing Method (ASTM D6752-02 and AASHTO T-331) refers to the Bulk Specific Gravity of compacted bituminous mixtures. The standards require that the resistant polymer bag and the sample be weighed individually. Then, the specimen is placed into the bag and placed inside the vacuum chamber, which is completely evacuated of air before the bag is automatically sealed. The bag tightly conforms to the specimen's surface and prevents the infiltration of water into the specimen. At this point, the sealed specimen is weighted in water, and once this weight is obtained, the bag is cut to allow the water to enter the specimen. Once also this weight is obtained, the bulk specific gravity and

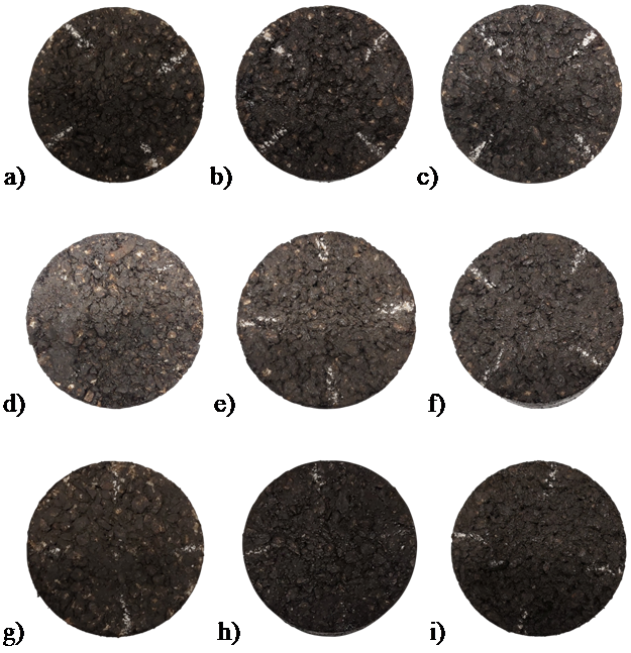

Note. AC6o_27_N75_0CR (a), AC6o_28_N75_0CR (b), AC6o_29_N75_0CR (c), AC6o_27_N50_0CR (d), AC6o_28_N50_0CR (e), AC6o_29_N50_0CR (f), AC6o_30_N75_2CR (g), AC6o_31_N75_2CR (h), AC6o_32_N75_2CR (i).

Figure 10: Top surface of samples

Table 5: Design of experiments

Mixtures	AC6o_27_N75_0CR	AC6o_27_N50_0CR	AC6o_28_N75_0CR	AC6o_28_N50_0CR	AC6o_29_N75_0CR	AC6o_29_N50_0CR	AC6o_30_N75_2CR	AC6o_31_N75_2CR	AC6o_32_N75_2CR
Sample gradation	See Figure 11a.								
Bitumen percentage (w/w by mixture weight)	3.20	3.20	5.70	5.70	7.20	7.20	3.00	5.50	7.00
Crumb rubber percentage (w/w by mixture weight)	0.00	0.00	0.00	0.00	0.00	0.00	2.00	2.00	2.00
Compaction (number of gyrations)	75	50	75	50	75	50	75	75	75
Tests	See Table 6, tests 1-7.								

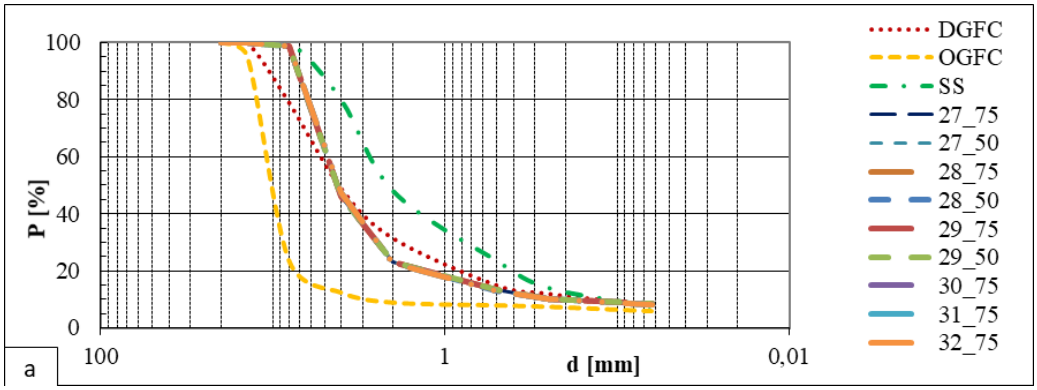

Symbols. DGFC: Dense-graded friction course. OGFC: Open-graded friction course. SS: Slurry seal. 27_75: AC6o_27_N75_0CR; 27_50: AC6o_27_N50_0CR; 28_75: AC6o_28_N75_0CR; 28_50: AC6o_28_N50_0CR; 29_75: AC6o_29_N75_0CR; 29_50: AC6o_29_N50_0CR; 30_75: AC6o_30_N75_2CR; 31_75: AC6o_31_N75_2CR; 32_75: AC6o_32_N75_2CR.

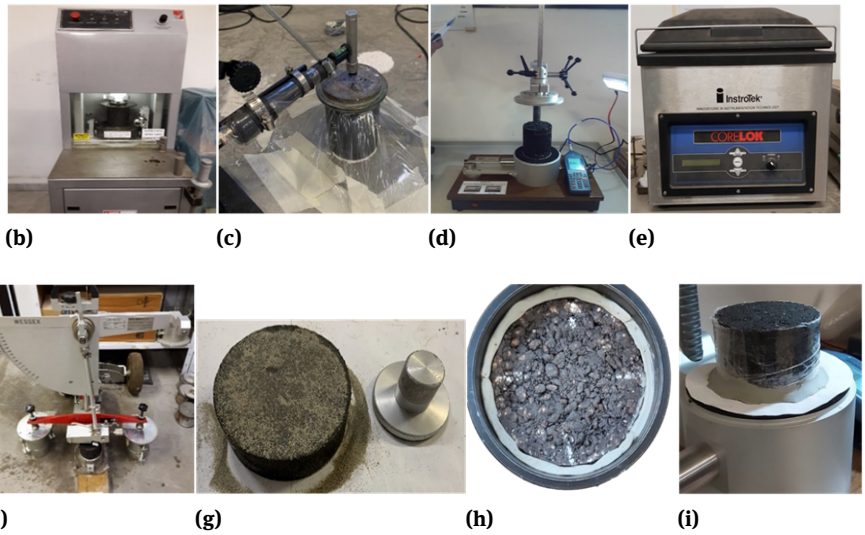

Note. Grading curve of the experimental mixtures with respect to dense-graded friction course, open-graded friction course and slurry seal curve (a), Superpave gyratory compactor (b), Impulse hammer (c), Airflow resistance meter (d), Corelok (e), Skid resistance tester (f), Sand patch tester (g), sealed samples in the Kundt tube (h) and in the airflow resistance meter (i).

Figure 11: Materials and devices

the porosity can be calculated as indicated by the standard.

5. Permeability (flexible wall permeameter, cf. ASTM PS 129-1, Figure 6). The Flexible Wall Permeameter is a falling-head permeameter used in the laboratory to measure the permeability coefficient of saturated asphalt concrete samples. The device consists of a vertical graduated cylinder, placed on the top of a cylindrical aluminium container equipped with a latex membrane, an air pump, a pressure gauge, and a valve to allow the water to flow out. Before the test, the sample is saturated inside a vacuum container, where the vacuum is created. After evacuating the air inside the vacuum container using the appropriate pump, the sample is sealed by pressurizing a latex membrane. The graduated cylinder is filled with water, leaving the flow valve open. At this point, the time interval required for the water level to decrease from an initial height h1 to a final height h2 inside the vertical graduated cylinder can be measured. According to the ASTM PS-129, the sample is considered saturated when 4 consecutive measurements do not differ by more than 10% from the average of the consecutive test results. Once sample saturation is verified, the final time measured is recorded and used to calculate the coefficient of water permeability at 20°C. The ASTM PS-129 (withdrawn in 2003) and the FM 5-565 may be used.
6. Skid resistance (pendulum tester, cf. EN 13036-4, [32], Figure 11f). The EN 13036-4 standard describes a

method for determining the Slip/Skid Resistance. The test is carried out by means of a slider mounted at the end of the pendulum swing arm, which glides over the surface at a given contact distance. The arm is placed horizontally with a pointer and when it is released, it swings and strikes the surface. Friction causes the arm to decelerate. The test is repeated 5 times and the average value is obtained. In accordance with ANAS requirements [30], the PTV values for type A surface course (draining surface courses) must be higher than 55.

7. Sand patch test (cf. EN 13036-1, ASTM E965, [33], Figure 11g). The Sand Patch Test is used to assess the mean texture depth, that is the average depth of texture below the peaks of the surface. A known quantity of sand is poured into a heap on the test surface. With light pressure, the sand is spread through a circular motion, using a sand spreader, until the sand is spread into a circular patch with the surface depression filled to the level of the peaks.

4 Results

Table 6 and 7 and Figure 12 illustrate the results.

Based on the values of the acoustic absorption coefficient obtained (Figure 12), it can be observed that all the specimens present a poor acoustic absorption: the values range from 0.05 to 0.25, while the maximum values correspond to the mixture AC6o_27_N50_0CR.

For the results, note that all the obtained values are similar, except that for the mixtures AC6o_27_N50_0CR and AC6o_32_N75_2CR, which present lower values. For airflow resistivity, values range from 774 kNs/m^4 to 1726 kNs/m^4. Note that these values comply with the reference values provided in the study [34], where, for dense-graded friction courses, values in the range 600–30,000 kNs/m^4 are

Table 6: Results of preliminary tests

Standard	ISO 10534-2	UNI EN ISO 053-1	EN 29052-1, ISO 7626-5	ASTM D6752-02, AASHTO T-331	ASTM D6752-02, AASHTO T-331	ASTM D6752-02, AASHTO T-331	EN 13036-4	ASTM PS 129-1, FM 5-565	EN 13036-1
Mixture	a_{oM}	r	MI	Gmb	P	AV	PTV	k_{20}	MTD
AC6o_27_N75_0CR	0.09	1,576k	319.0	2.349	7.74	9.96	73	0.004	0.430
AC6o_27_N50_0CR	0.25	597k	53.6	2.197	13.91	15.77	62	0.041	0.481
AC6o_28_N75_0CR	0.06	1,252k	323.0	2.391	2.81	4.65	70	-	0.515
AC6o_28_N50_0CR	0.11	1,051k	143.0	2.272	7.19	9.39	71	0.012	0.628
AC6o_29_N75_0CR	0.05	1,727k	155.0	2.399	1.50	2.10	65	-	0.537
AC6o_29_N50_0CR	0.08	1,606k	246.0	2.328	3.55	5.00	75	0.001	0.545
AC6o_30_N75_2CR	0.12	1,657k	58.6	2.257	9.47	11.03	74	0.005	0.162
AC6o_31_N75_2CR	0.06	1,315k	50.1	2.309	2.88	5.40	75	-	0.444
AC6o_32_N75_2CR	0.07	774k	126.0	2.305	7.19	3.44	75	0.002	0.918
Expected range for porous asphalts	> 0.25–0.50 [30]	1k – 60k [34]	40–100 [35]	(2)	-	≥ 22 (N_{des} = 50) ≥ 21 (N_{des} = 75) (3) [30]	≥ 55 [30]	≥ 0.18 [30, 36]	> 1.0 [34]
Expected range for dense-graded friction courses	-	600k – 30,000k [34]	80 – 100 [37]	(2)	-	≥ 9 (N_{des} = 50) ≥ 7 (N_{des} = 75) (3) [30]	≥ 55 [30]	< 0.18 [30, 36]	0.4 – 1 [34]

Notes

(2) Gmb values depend on the type of aggregates used, the type of bitumen and the degree of compaction.

(3) Values obtained through interpolation of the values provided by the ANAS requirements [30].

Symbols: aoM: Mean acoustic absorption coefficient (200<f<1600 Hz) [-]. r: Airflow resistivity [kNs/m4]. MI: max Mechanical impedance [kNs/m]. Gmb: Bulk specific gravity [-]. P: Porosity [%]. AV: air voids [%]. PTV: Pendulum test value [-]. k20: Coefficient of water permeability at 20°C [cm/s]. MTD: Mean texture depth [mm].

Table 7: Correlation matrix among measured parameters

	a_{oM}	r	MI	Gmb	P	AV	PTV	k_{20}	MTD
a_{oM}	1								
r	−0.56	1							
MI	−0.40	0.34	1						
Gmb	−0.83	0.59	0.69	1					
P	0.93	−0.41	−0.34	−0.83	1				
AV	0.91	−0.36	−0.30	−0.81	0.98	1			
PTV	−0.58	0.31	0.13	0.14	−0.38	−0.34	1		
k_{20}	0.97	−0.66	−0.40	−0.77	0.85	0.83	−0.68	1	
MTD	−0.25	−0.54	0.12	0.15	−0.38	−0.46	0.04	−0.07	1

Note. Symbols are given in Table 6.

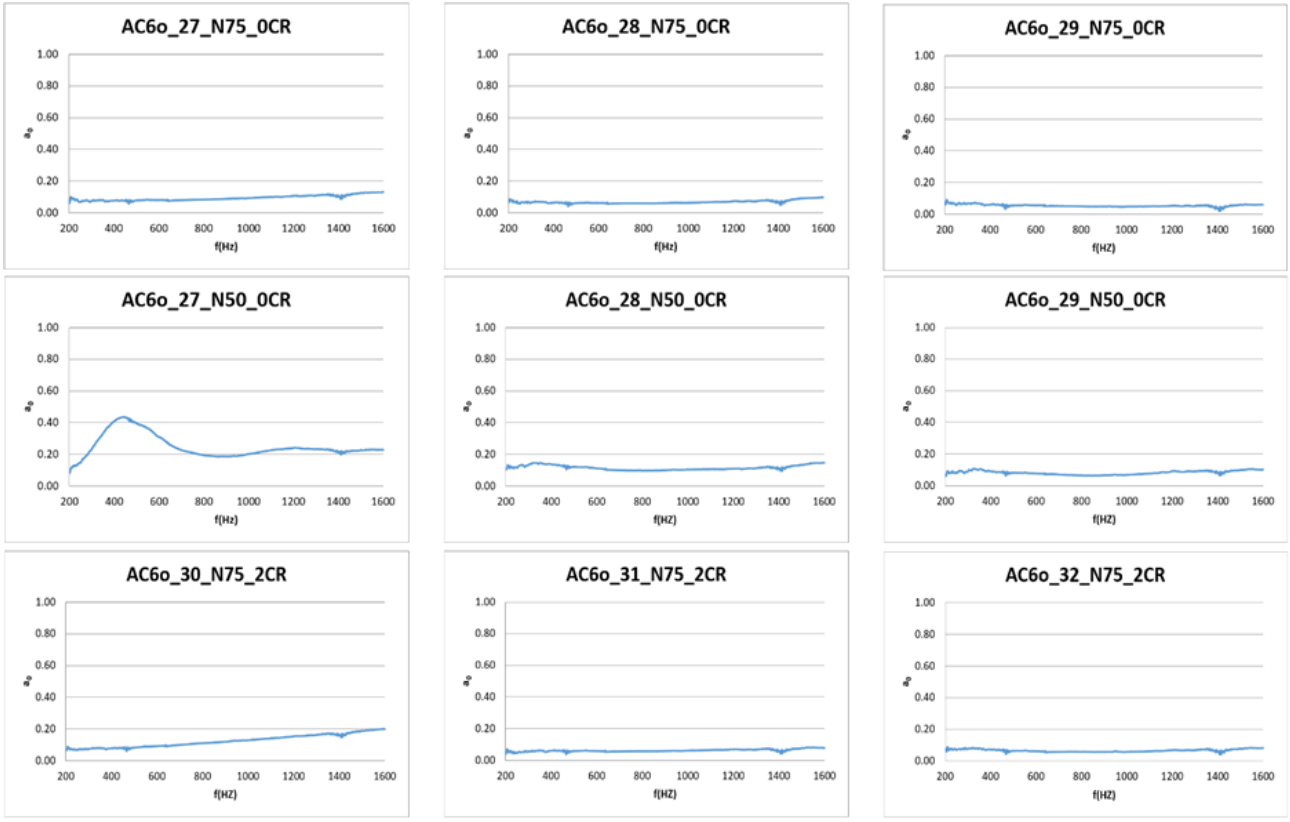

Figure 12: Sound absorption coefficients

foreseen, while, for open-graded friction courses, airflow resistivity ranges from 1 to 60 kNs/m^4.

Analysing the values of mechanical impedance obtained, it emerges that the AC6o_28_N75_0CR (without rubber) presents the highest value, while the AC6o_31_N75_2CR (with CR) has the lowest value. Overall, it can be deduced that bitumen percentage and crumb rubber percentage affect the mechanical impedance.

Comparing the percentages of air voids obtained with the limits imposed by ANAS requirements [30], it emerges that the percentages obtained are lower than the values required for porous mixtures (≥ 22%), but higher than the ones that refer to dense-graded friction courses at Ndes (3–6%).

In accordance with ANAS requirements [30], MTD must be higher than 0.4 mm for surface courses. This limit is respected for all the samples, with the exception of AC6o_30_N75_2CR.

Pearson's correlation coefficients are shown in Table 7 (where +1 corresponds to perfectly positive linear

correlation, 0 corresponds to no linear correlation, and –1 corresponds to perfectly negative linear correlation). By analysing the values of the matrix, it can be seen that (cf. Figure 13):

- a_{0M} has a strong correlation with *Gmb, P, AV*, and k_{20};
- G_{mb} has a strong correlation with *P*, *AV*, and k_{20};
- *P* has a strong correlation with *AV* and k_{20};
- *AV* has a strong correlation with k_{20}.

5 Discussion

Figures 13 and 14 highlight the connection between the main parameters discussed in this study. Sensors and devices are described in Sections 1.5, 1.6, 1.8.

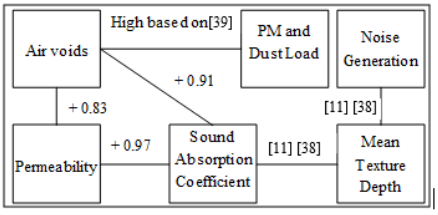

Figure 13: Correlation between main parameters

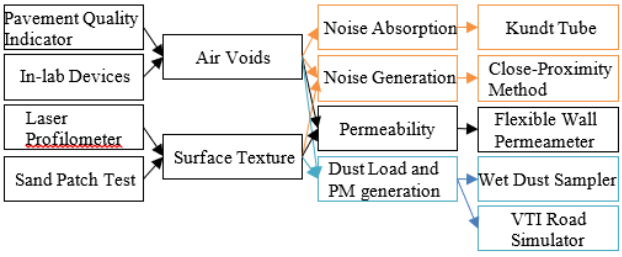

Figure 14: Sensor system, parameter, and performance

5.1 Acoustics versus PM resuspension and dust load

Acoustics is affected by air voids, in terms of air void percentage, tortuosity, pore shape factors, and air void-related parameters such as resistivity [38]. Higher air void contents yield higher acoustic absorption coefficients, as seen above. On the other hand, PM resuspension and dust loads are affected by surface texture and air voids [39]. Higher air void percentages seem to cause higher production of PM but also seem to correspond to higher dust load capabilities [39]. The acoustic absorption is also related to the surface texture (*e.g.*, texture spectra levels such as L16 to L630) which may increase determining the increase of the rolling noise especially in the frequency components lower than 1 kHz (cf. [40]). As the air void percentage increases, the maximum acoustic absorption coefficient and the peak frequency increases [38]. In summarising, both noise-related factors and PM-related factors depend on AV and surface texture and this seems to be a good starting point for future research.

5.2 Acoustics versus permeability

Sound absorption also depends on pore connectivity, and constraints in the pore network through which acoustic energy can travel and attenuate within the material [38]. The maximum absorption coefficient increases with increasing pore connectivity [38, 41]. Also, as the pore size and connectivity increase, water will pass through the material much faster and as a result the permeability coefficient will have a higher value [38]. Results in Table 6 confirm this observation. Consequently, acoustics and permeability both depend on AV and their relationship appears strong and physically based.

5.3 Permeability versus PM resuspension and dust load

The clogging process over time affects the permeability of the material, being understood as a reduction in functionality [42]. In particular, clogging occurs due to the accumulation of suspended particles, mainly due to vehicular traffic and therefore to the wear of mechanical components, to the interaction between tire and pavement, but also due to

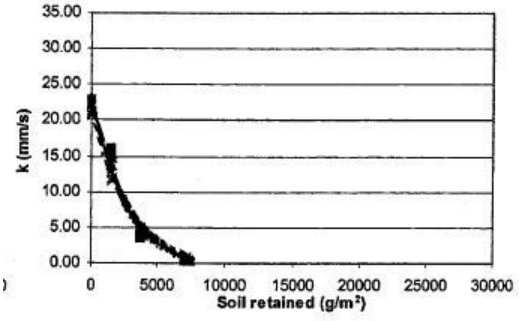

Figure 15: Content of soil retained vs. permeability [43]

atmospheric agents, such as rain and wind, which cause their resuspension.

This points out that dust load, which is responsible for clogging, affects permeability.

6 Conclusions

Based on the data and the studies carried out, the following conclusions can be drawn:

- Noise mapping and permeability mapping often depend on a common factor, which is the air void content. This conceptual analogy fails when considering texture-optimised pavements, where the noise mitigation is obtained through texture optimisation instead of through absorption optimisation. The results obtained in this study confirm this dependency and point out that permeability mapping could be used as a proxy of noise mapping for several types of pavements.
- For PM production and dust load, the studies in the literature point out that the dust load is well correlated with air voids. This seems to confirm that the dust load could be predicted through noise or permeability mapping. For PM generation, the studies in the literature highlight that higher texture depths could yield higher PM production factors. Consequently, this could cause higher resuspension phenomena. Overall, while between noise and permeability (for porous asphalts) a strong correlation appears to be given, for PM-related mapping and other thematic maps more studies are needed.
- Based on the results in the literature, it is predicted that as clogging (and dust load) increases, porosity decreases, affecting the other characteristics. In particular, as clogging increases, the value of the sound absorption coefficient undergoes a drastic reduction.
- Further studies are needed to investigate the relationship between PM-related indicators and phenomena (dust load and resuspension) versus noise mapping.
- Further studies are needed to focus in more detail the consequences deriving from having such an added and supplementary use of noise maps (PM- and permeability-related maps. This includes issues in terms of noise mapping prediction through codes. To this end, a case study will be designed and discussed.

For future research, it is planned to apply a new laboratory procedure to study the change in permeability and sound absorption by subjecting the samples to clogging cycles with sand and heavy metals, in order to better evaluate the correlation between sound absorption and permeability, affected by clogging. Future research will focus also on PM dust load quantification.

Funding information: The authors state no funding involved.

Author contributions: All authors have accepted responsibility for the entire content of this manuscript and approved its submission.

Conflict of interest: The authors state no conflict of interest.

References

[1] Lesieur A, Mallet V, Aumond P, Can A. Data assimilation for urban noise mapping with a meta-model. Appl Acoust. 2021 Jul;178:107938.
[2] Van Hauwermeiren W, Filipan K, Botteldooren D, De Coensel B. Opportunistic monitoring of pavements for noise labeling and mitigation with machine learning. Transp Res Part D Transp Environ. 2021 Jan;90:102636.
[3] Morley DW, de Hoogh K, Fecht D, Fabbri F, Bell M, Goodman PS, et al. International scale implementation of the CNOSSOS-EU road traffic noise prediction model for epidemiological studies. Environ Pollut. 2015 Nov;206:332–41.
[4] Tie SF, Tan CW. A review of energy sources and energy management system in electric vehicles. Renew Sustain Energy Rev. 2013 Apr;20:82–102.
[5] Wu Y, Zhang L. Can the development of electric vehicles reduce the emission of air pollutants and greenhouse gases in developing countries? Transp Res Part D Transp Environ. 2017 Mar;51:129–45.
[6] Timmers VR, Achten PA. Non-Exhaust PM emissions from battery electric vehicles. Non-Exhaust emissions. Elsevier; 2018. pp. 261–87.
[7] Czuka M, Pallas MA, Morgan P, Conter M. Impact of potential and dedicated tyres of electric vehicles on the tyre-road noise and connection to the EU noise label. Transp Res Procedia. 2016;14:2678–87.
[8] Campello-Vicente H, Peral-Orts R, Campillo-Davo N, Velasco-Sanchez E. The effect of electric vehicles on urban noise maps. Appl Acoust. 2017 Jan;116:59–64.
[9] Vázquez VF, Paje SE. Study of the road surface properties that control the acoustic performance of a rubberised asphalt mixture. Appl Acoust. 2016 Jan;102:33–9.
[10] Vaitkus A, Andriejauskas T, Vorobjovas V, Jagniatinskis A, Fiks B, Zofka E. Asphalt wearing course optimization for road traffic noise reduction. Constr Build Mater. 2017 Oct;152:345–56.
[11] Praticò FG, Briante PG. Prediction of surface texture for better performance of friction courses. Constr Build Mater. 2020 Jan;230:116991.

[12] Alves CA, Vicente AM, Calvo AI, Baumgardner D, Amato F, Querol X, et al. Physical and chemical properties of non-exhaust particles generated from wear between pavements and tyres. Atmos Environ. 2020 Mar;224:117252.
[13] Praticò FG, Briante PG. Particulate matter from non-exhaust sources. 11th international conference Environmental Engineering; 2020 May 21-22; Vilnius Gediminas Technical University, Lithuania. VGTU Technika; 2020. https://doi.org/10.3846/enviro.2020.622.
[14] Amato F, Favez O, Pandolfi M, Alastuey A, Querol X, Moukhtar S, et al. Traffic induced particle resuspension in Paris: emission factors and source contributions. Atmos Environ. 2016 Mar;129:114–24.
[15] Milne A, Landing W, Bizimis M, Morton P. Determination of Mn, Fe, Co, Ni, Cu, Zn, Cd and Pb in seawater using high resolution magnetic sector inductively coupled mass spectrometry (HR-ICP-MS). Anal Chim Acta. 2010 Apr;665(2):200–7.
[16] Odobašić A, Šestan I, Begić S. Biosensors for determination of heavy metals in waters. Biosensors for environmental monitoring. IntechOpen; 2019. https://doi.org/10.5772/intechopen.84139.
[17] Urrutia-Goyes R, Hernandez N, Carrillo-Gamboa O, Nigam KD, Ornelas-Soto N. Street dust from a heavily-populated and industrialized city: evaluation of spatial distribution, origins, pollution, ecological risks and human health repercussions. Ecotoxicol Environ Saf. 2018 Sep;159:198–204.
[18] Zannoni D, Valotto G, Visin F, Rampazzo G. Sources and distribution of tracer elements in road dust: the Venice mainland case of study. J Geochem Explor. 2016 Jul;166:64–72.
[19] Polukarova M, Markiewicz A, Björklund K, Strömvall AM, Galfi H, Andersson Sköld Y, et al. Organic pollutants, nano- and microparticles in street sweeping road dust and washwater. Environ Int. 2020 Feb;135:105337.
[20] Lundberg J, Blomqvist G, Gustafsson M, Janhäll S, Järlskog I. Wet dust sampler—a sampling method for road dust quantification and analyses. Water Air Soil Pollut. 2019 Jul;230(8):180.
[21] Pirjola L, Parviainen H, Hussein T, Valli A, Hämeri K, Aaalto P, et al. "Sniffer" a novel tool for chasing vehicles and measuring traffic pollutants. Atmos Environ. 2004 May;38(22):3625–35.
[22] Etyemezian V, Kuhns H, Nikolich G. Precision and repeatability of the TRAKER vehicle-based paved road dust emission measurement. Atmos Environ. 2006 May;40(16):2953–8.
[23] Hetem I, Andrade M. Characterization of fine particulate matter emitted from the resuspension of road and pavement dust in the metropolitan area of São Paulo, Brazil. Atmosphere (Basel). 2016 Feb;7(3):31.
[24] Amato F, Pandolfi M, Alastuey A, Lozano A, Contreras González J, Querol X. Impact of traffic intensity and pavement aggregate size on road dust particles loading. Atmos Environ. 2013 Oct;77:711–7.
[25] Amato F, Schaap M, Denier van der Gon HA, Pandolfi M, Alastuey A, Keuken M, et al. Short-term variability of mineral dust, metals and carbon emission from road dust resuspension. Atmos Environ. 2013 Aug;74:134–40.
[26] Jonsson P, Blomqvist G, Gustafsson M. Wet dust sampler technological innovation for sampling particles and salt on road surface. Fourth National Conference on Surface Transportation Weather; Seventh International Symposium on Snow Removal Symposium on Snow Removal; 2008 Jun 16-19; Indianapolis, USA. 2008 p. 102-111.
[27] Ranieri V, Colonna P, Sansalone JJ, Sciddurlo A. Measurement of hydraulic conductivity in porous mixes. Transp Res Rec. 2012 Jan;2295(1):1–10.
[28] Li H, Kayhanian M, Harvey JT. Comparative field permeability measurement of permeable pavements using ASTM C1701 and NCAT permeameter methods. J Environ Manage. 2013 Mar;118:144–52.
[29] Chen LM, Chen JW, Chen TH, Lecher T, Davidson P. Measurement of permeability and comparison of pavements. Water. 2019 Mar;11(3):444.
[30] ANAS S.p.A. Capitolato speciale di appalto - norme tecniche per l'esecuzione del contratto. 2016;2.
[31] Praticò GF. Roads and loudness: a more comprehensive approach. Road Mater Pavement Des. 2001 Dec;2(4):359–77.
[32] Praticò FG, Astolfi A. A new and simplified approach to assess the pavement surface micro- and macrotexture. Constr Build Mater. 2017 Sep;148:476–83.
[33] Praticò FG. Quality and timeliness in highway construction contracts: a new acceptance model based on both mechanical and surface performance of flexible pavements. Construct Manag Econ. 2007 Mar;25(3):305–13.
[34] Praticò FG, Vizzari D, Fedele R. Estimating the resistivity and tortuosity of a road pavement using an inverse problem approach. 24th International Congress on Sound and Vibration; 2017 Jul 23-27; London, UK. 2017.
[35] Radenberg M, Drewes B, Manke R. Noise reducing effect of new dense asphalt layers. 6th Eurasphalt & Eurobitume Congress. 2016 Jun 1-3; Prague, Czech Republic. 2016.
[36] Praticò FG, Moro A. Permeability and volumetrics of porous asphalt concrete. A theoretical and experimental investigation. Road Mater Pavement Des. 2007 Nov;8(4):799–817.
[37] Pratico FG, Pellicano G, Fedele R. The study of road pavement performance through impact hammer tests. 11th international conference "environmental engineering"; 2020 May 21-22; Vilnius Gediminas Technical University, Lithuania. VGTU Technika; 2020.
[38] Neithalath N, Weiss J, Olek J. Characterizing Enhanced Porosity Concrete using electrical impedance to predict acoustic and hydraulic performance. Cement Concr Res. 2006 Nov;36(11):2074–85.
[39] Chen J, Wang W, Liu H, Ren L. Determination of road dust loadings and chemical characteristics using resuspension. Environ Monit Assess. 2012 Mar;184(3):1693–709.
[40] Kragh J, Møller Iversen L, Sandberg U. Road surface texture for low noise and low rolling resistance. Norway: Vejdirektoratet Rapport 506. 2013.
[41] Liao G, Sakhaeifar MS, Heitzman M, West R, Waller B, Wang S, et al. The effects of pavement surface characteristics on tire/pavement noise. Appl Acoust. 2014 Feb;76:14–23.
[42] Singh A, Sampath PV, Biligiri KP. A review of sustainable pervious concrete systems: emphasis on clogging, material characterization, and environmental aspects. Constr Build Mater. 2020 Nov;261:120491.
[43] Tan SA, Fwa TF, Han CT. Clogging evaluation of permeable bases. J Transp Eng. 2003 May;129(3):309–15.